M=1 and 2 Gravitational Instabilities in Gaseous Disks: I. Diffuse Gas

S. Junqueira[1,2] and F. Combes[1]

[1] DEMIRM, Observatoire de Paris, 61 Av. de l'Observatoire, F–75014, Paris, France
[2] CNPq-Observatório Nacional, DAGE, R. Gal. José Cristino 77, CEP 20921–400, Rio de Janeiro, Brazil

February 1, 2008

Abstract. We report the results of self-gravitating simulations of spiral galaxies, modeled by stellar and gaseous components, developed to investigate in particular the role of dissipation in the evolution of galaxy disks. The gas disk is simulated by the Beam-Scheme method, where it is considered as a self-gravitating fluid. The results suggest that the gravitational coupling between the stars and gas plays a fundamental role in the formation and dissolution of stellar bars, depending on the gaseous mass concentration and on the degree of dissipation. In addition we remark that initially concentrated gas disks can be unstable to the one-armed (m=1) spiral perturbations, which may explain the lopsided features observed in the gas distribution of the late-type isolated galaxies. The development of the m=1 feature slows down the radial gas flows towards the center, since the large-scale gravity torques are then much weaker.

Key words: Galaxies: evolution; Galaxies: general; Galaxies: ISM; Galaxies: kinematics & dynamics; Galaxies: spiral; Galaxies: structure

1. Introduction

While the gravitational instabilities of a purely stellar disk have been widely studied, mainly through simulations, and begin to be well understood, the situation is much more open for a self-gravitating disk composed of stars and gas. Even when a stellar disk is stabilised against axisymmetric instabilities (Toomre criterion, 1964), it can be the site of spiral and bar instability (e.g. Sellwood & Wilkinson 1993), together with z-instabilities (e.g. Combes et al 1990). These heat considerably the stellar disk, that can then no longer sustain spiral structure. Instabilities can be suppressed by reducing the effective self-gravity of the stellar disk, either through the addition of a hot bulge or halo (Ostriker & Peebles 1973), or through disk heating, i.e. increasing the velocity dispersion (Athanassoula & Sellwood 1986).

The behaviour of a self-gravitating disk of both stars and gas, even if the latter represents only a few percents of the total mass, presents much more variety and complexity. Due to the dissipation, the gaseous component remains cool, and evacuates the heating due to the gravitational instabilities: spiral structure can then be continuously renewed (e.g. Sellwood & Carlberg 1984), even in the stellar disk. Criteria for stability are more complex, the gravitational coupling between gas and stars making the ensemble unstable, even when each component would have been separately stable (e.g. Jog & Solomon 1984, Bertin & Romeo 1988, Elmegreen 1994). Gravity torques exerted on the gas produce strong radial flows, and gas can accumulate at Lindblad resonances and form several rings (e.g. Schwarz 1981, Combes 1988). The strong gas concentration in the nucleus can destroy stellar bars (Friedli & Benz 1993), after having sometimes triggered a nuclear bar within the main one (Friedli & Martinet 1993). This bar destruction can be explained by an increase of chaotic orbits in the stellar bar (Hasan & Norman 1990). The copious inflow of gas into the nuclear region may be one of the main source of nuclear activity in galaxies (Phinney, 1994).

When the gas possess too much self-gravity, however, it forms lumps through Jeans instability, and the lumpiness of the gas can scatter the stars, randomize their motions, and prevent any bar formation (Shlosman & Noguchi 1993). While the gas is triggering bar instability when it represents only a few percents of the total mass, it can play the inverse role when its mass is above $\approx 10\%$.

All the complexity of the evolution of a self-gravitating galaxy disk composed of stars and gas has not yet been explored; moreover, the detailed physics of the interstellar medium has not yet be quantified: we still do not know the exact amount of dissipation, or the energy balance between dissipation and star formation, etc.. We want to

study to what extent the galaxy evolution depends on these parameters, through the gas behaviour. We want to compare the behaviour of the two main gas phases, condensed and diffuse.

Observations show that the gas component is a multiphase medium, spanning a wide range of densities and temperatures. To drastically simplify, we can consider two distinct forms - dense, cold and clumpy molecular clouds and warm diffuse gas - with different spatial distribution but having comparable total masses. The two aspects of the gas component have been studied in the literature: ensembles of interstellar clouds that undergo collisions, but do not behave as a fluid (Schwarz 1981, 1984; Roberts & Hausman 1984; Combes & Gerin 1985). The collisions take place mainly along spiral arms. This method describes essentially the molecular gas component. The response of the diffuse gas in barred potentials was also explored (Huntley et al 1978; Roberts et al. 1979; Sanders & Tubbs 1980; van Albada & Sanders 1982; Prendergast 1983; van Albada 1983; Contopoulos et al. 1989). In these calculations the gas was considered as a fluid, submitted to pressure forces, and undergoing shocks. In most cases, the gas self-gravity was not considered.

In the present paper we concentrate on the self-gravitating diffuse phase, and present numerical simulations of spiral galaxies modeled by two components, stars and gas-fluid. The primary motivation is to quantify the amount of dissipation (either artificial, turbulent or "gravitational") and radial flow of the gas in the formation and evolution of the gravitational instabilities observed in spiral disks. In particular we discuss phenomena that can be explained by the star-gas coupling. Future studies will compare the condensed with the diffuse phase behaviour, and will study a combination of the two.

This paper is organized as follows. In § 2 we discuss the computational methods, the galaxy model used and the initial conditions of our simulations. In § 3 we present the results concerning the m=2 instabilities, and in § 4 the m=1 and one-armed spiral instabilities. Section 5 quantifies the effects of viscosity and section 6 summarizes our conclusions.

2. Numerical Simulations

2.1. Computational Methods

We simulate the self-gravity of both the stellar and gaseous components, and solve the N-body problem by the 2D-Fast Fourier Transforms method. At each integration step, density (of stars and gas) is computed at each point of a grid of 256×256 square cells. Fourier transform of density and inverse transform of potential are then carried out. The potential is softened within 250 pc, which is also the cell size. Each particle contributes to the density of the four nearest grid points, according to cloud-in-cell (CIC) interpolation procedure (Birdsall & Fuss 1969). There are

36000 particles representing the stellar component. The gaseous component is represented by a fluid.

The fluid is simulated according to the Beam-Scheme method developed by Sanders & Prendergast (1974). This technique for solving the hydrodynamical equations, is an explicit Eulerian scheme. The gas is evolved on a 256×256 2D-Cartesian grid, with mass, momentum, and energy densities being specified in each cell. The presumed Maxwellian velocity distribution in each gas cell is approximated by five delta functions (or beams), which reproduce the appropriate moments of the velocity distribution function. These beams are allowed to move over a time step transporting mass, momentum and energy into adjacent gas cells. Transport is taken into account to determine the new mass, momentum, and energy in each cell, and these moments are used to describe the new Gaussian velocity distributions for each cell of the gas.

2.2. Galaxy Model

As for the initial conditions, the model galaxy is composed of a stellar disk, an analytical spherical bulge and a gaseous disk. The stellar particles are initially distributed according to a Toomre disk (Toomre, 1962) of mass M_d and radial scale length a_d. The gaseous component of mass M_g is modeled by another Toomre disk, of radial scale length a_g, with velocities distributed in beams according to the Beam-Scheme method. A Plummer potential (Binney & Tremaine 1987) of radial scale length a_b, represents the bulge. In all simulations the bulge and the disk have the same mass ($M_d = M_b$) and the gas mass corresponds to 10% of the total mass of the galaxy ($M_g = 0.1M_t$; $M_t = 10^{11} M_\odot$). The initial cutoff radius of the stellar and gaseous disks are 12 kpc and 16 kpc, respectively. The characteristic scale of the stellar disk, of the bulge and of the gaseous disk are free parameters. Their values are shown in Table 1. Initially, the stellar particles have a velocity dispersion as a function of radius corresponding to the Toomre parameter $Q = 1$ all over the disk. The rotational velocity is corrected for asymmetric drift. The units of time, distance and mass for all simulations are 10^7 years, 1 kpc and $4 \times 10^9 M_\odot$ respectively. All the experiments have been evolved through a total time equal to 2.2×10^9 years. The time-step is 0.1 unit= 1 Myrs.

In the experiments A, B, C and D the gaseous component is not included. These are control simulations in order to probe the gas influence. In the E, F, G and H experiments the stellar components are described by the same initial conditions as in the A, B, C and D experiments but a gaseous disk, of scale length $a_g = 6$ kpc, is included. A comparative analysis of these experiments allow us to draw important conclusions about star-gas coupling. Experiments I and J test the role of the initial concentration of the gaseous disk in the evolution of the system.

Table 1. Parameters of the Experiments

Exp.	a_d	a_b	a_g
A	3.0	1.0	
B	4.5	1.0	
C	3.0	2.0	
D	4.5	2.0	
E	3.0	1.0	6.0
F	4.5	1.0	6.0
G	3.0	2.0	6.0
H	4.5	2.0	6.0
I	3.0	1.0	4.0
J	3.0	1.0	8.0

3. M=2 instabilities

In this section we discuss the role of gas dissipation in the formation and maintenance of gravitational instabilities ($m = 2$ spirals, bars).

3.1. Influence of the gas

In figure 1 we present the linear isodensity contours of the stars for the experiments A, B, C and D at the time t=140 (10^7 yrs). In these four experiences, as described in the preceding section, the gaseous component is not included. We can note that in spite of the large bulge mass ($M_d = M_b$) a central bar develops. The spiral arms formed initially are only transient. They help to transfer angular momentum outwards to make the bar grow. The characteristic time-scale for bar formation in these experiments varies according to the degree of concentration of the initial bulge and stellar disk. Models with a smaller bulge scale length a_b, developed their bar in a shorter time-scale than those with a larger initial value of a_b. This can be checked by comparing experiments A and C or the experiments B and D, and can be interpreted by a shorter dynamical time-scale in the center of A and C. The bar is also shorter in length in Exp. A and C, and the corotation radius is smaller. Considering now the same initial mass concentration for the bulge (experiments A and B) we verify that disks initially more concentrated (experiment A) allow a more rapid bar formation. This could be due to the larger self-gravity of the stellar disk in the center, together with the shorter t_d there.

The main conclusion from these four experiments is the high longevity of the bar: the bar kept its amplitude up to the end of simulations (2.2 Gyrs). In the absence of gas, bars are long-lived, even in the presence of a concentrated bulge.

On the contrary, a great variety of scenarios can occur when the gaseous component is included. In figures 2, 3, 4 and 5 we present the linear isodensity contours of the stars and gas for the experiments E, F, G and H, at four different epochs (t=20, 80, 140 and 200 $\times$ 10^7 yrs). In

these experiments, the stellar and gaseous components can develop a bar (experiment E), in the same way as pure stellar runs, or evolve to various degrees of central mass concentration (Exp. F, G and H). In that case either the bar forms, and is then destroyed rapidly (experiments G and H) or even the bar does not form at all (experiment F).


Fig. 1. Exp. A, B, C and D: linear isodensity contours of the stars at epoch t=140 (in 10^7 yrs). X and Y are in kpc.
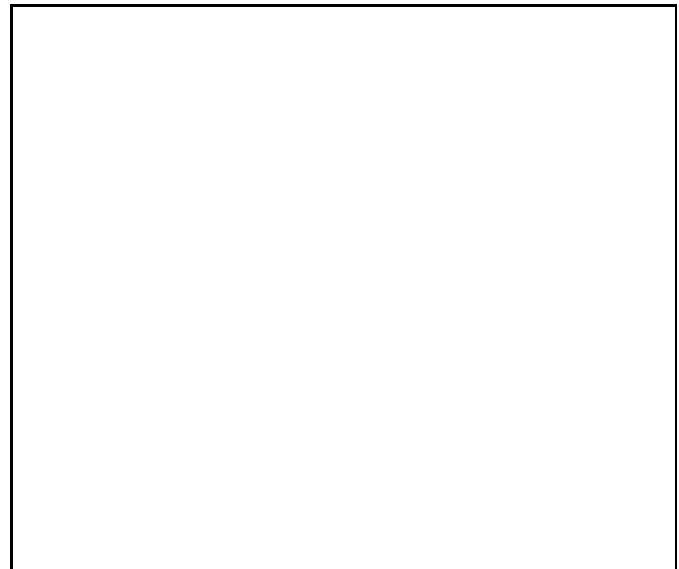
Fig. 2. Exp. E: linear isodensity contours of the stars (left side) and of the gas (right side) at epochs t=20, 80, 140 and 200 (in 10^7 yrs). X and Y are in kpc.
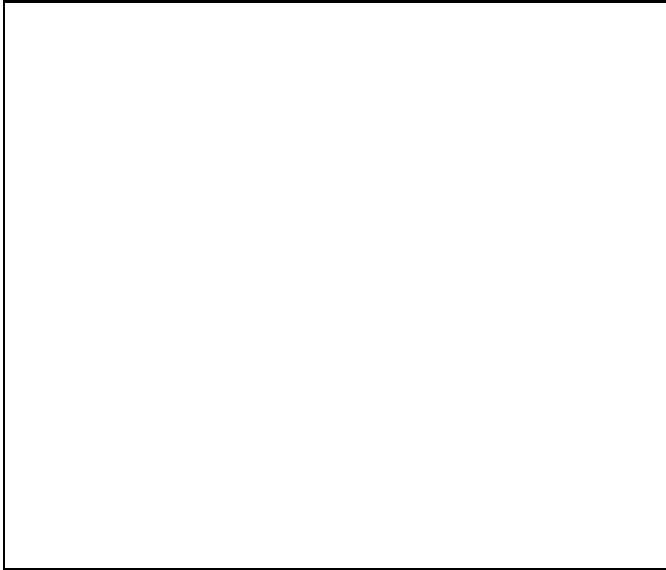
Fig. 3. Exp. F: linear isodensity contours of the stars (left side) and of the gas (right side) at epochs t=20, 80, 140 and 200 (in 10^7 yrs). X and Y are in kpc.
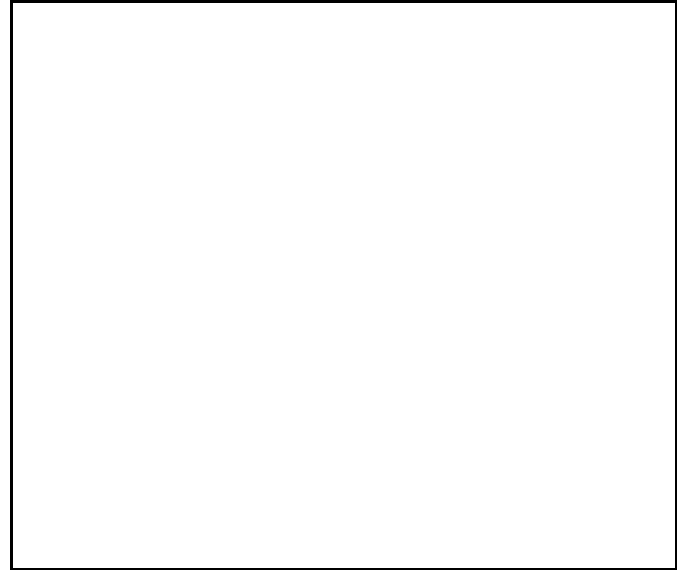
Fig. 5. Exp. H: linear isodensity contours of the stars (left side) and of the gas (right side) at epochs t=20, 80, 140 and 200 (in 10^7 yrs). X and Y are in kpc.
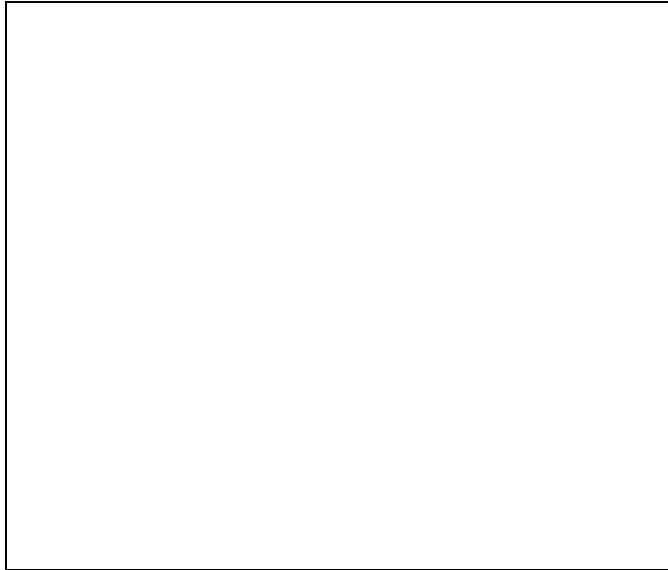
Fig. 4. Exp. G: linear isodensity contours of the stars (left side) and of the gas (right side) at epochs t=20, 80, 140 and 200 (in 10^7 yrs). X and Y are in kpc.

3.2. Bar amplitude and pattern speed

As described above, the bar strength and evolution depends on the central mass concentration and the gas fraction. We focus in this section on the bar evolution, the results of the experiment F where a central mass concentration is obtained without the formation, even transient, of a bar will be discussed in the next section.

To better identify the $m = 2$ perturbation, we have computed, for all simulations, the angular velocity of the pattern Ω_p as a function of radius. A mode would be characterized by a constant Ω_p over a range of radii. A Fourier analysis of the density distribution or of the potential allows to decompose the perturbation present in the galaxy in several components (m). The index m indicates the symmetry of each component or, in the case of spirals, the number of arms. The analysis provides, at each epoch, both the strength or amplitude of the m component, which growth rate can then be estimated and its phase, from which $\Omega_p(r)$ can be derived. We have computed the growth rate for the spiral-bars in the experiments A, E, G and H assuming exponentially growing modes. The behavior of the bar amplitude, the maximum ratio of the $m = 2$ tangential force to the radial force (p_2) as a function of time is shown in figure 6. While for the experiments A and E p_2 remains approximately constant as in a steady-state (although the bar weakens somewhat in experiment E), in experiments G and H it decreases rapidly. The growth time-scales obtained for the bars are approximately 7 t_d (Exp. A), 6 t_d (Exp. E), 5 t_d (Exp. G) and 4 t_d (Exp. H) where t_d is the dynamical time scale ($\approx 4 \times 10^7$ yrs). We remark that in Exp. A and E the behavior of p_2 in the first instants of the simulation (before the exponential bar growth) indicates the presence of transient spiral structure preceding bar formation. We have calculated for the experiments A and E the angular velocity (or pattern speed) $\Omega_p(r)$ for the bar perturbation. In figure 7 are shown the Ω (solid curve), $\Omega + \kappa/2$

and $\Omega - \kappa/2$ (dashed curves) frequency curves, where κ represents the epicyclic frequency and Ω is the angular velocity of the galaxy. The expected position of the Lindblad resonances are indicated at the top. It can then be noted that the bars are confined within their corotation radius in both experiments.

Fig. 6. The strength of the bar perturbation p_2 as a function of time (in 10^7 yrs units) for the experiments A, E, G and H. The m=2 amplitude has been averaged over radius 0 to 5kpc.
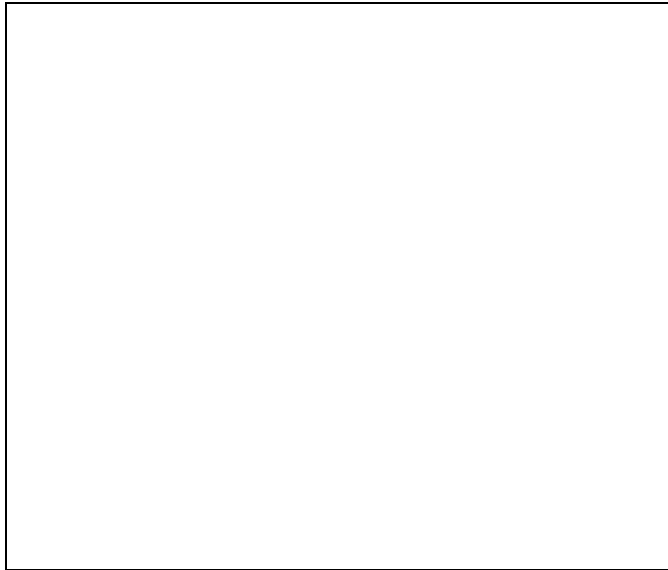
Fig. 7. The frequency curves (in units of 100 km/s/kpc) as a function of radius (in kpc) and the position of the pattern speed $\Omega_p(r)$ for experiments A (top) and E (bottom).
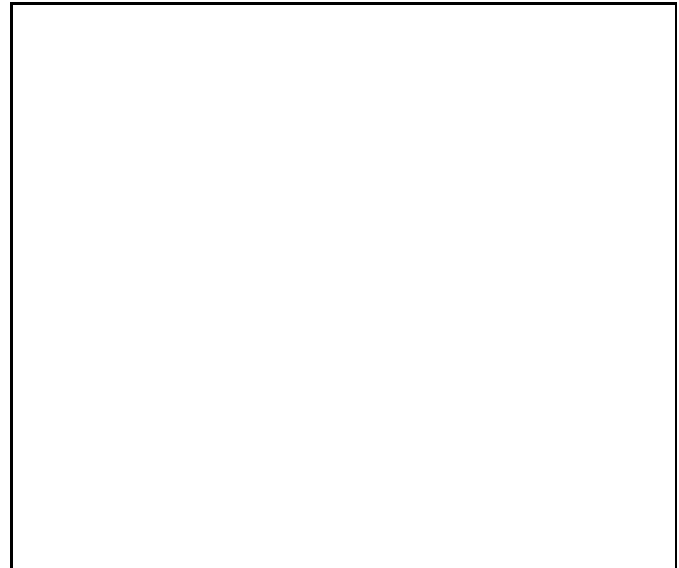
Fig. 8. Exp. E, F, G and H : surface density (in code units) of the stars and gas as a function of radius (in kpc) at four different epochs t=20, 80, 140 and 200 (in 10^7 yrs). The letters at the bottom left corner of each figure indicate (s) stars and (g) gas.

Figure 8 displays the evolution of the surface density of stars (left side) and gas (right side), as a function of radius, at four different epochs. These quantify the consequences of radial gas flows and mass concentration of stars and gas in the central region. Radial flows correspond to angular momentum transfer driven by non-axisymmetric gravitational instabilities, and the subsequent central mass concentrations react back on gravitational instabilities.

As is apparent in figure 8, in all simulations the surface density of stars still follows, at the first epoch (t=20), the imposed initial conditions. On the contrary, the gas surface density is determined at the first epoch, by the bulge mass concentration. Such behavior determines the future evolution of the stellar density distribution. In other words, at t=20 the gas, in the experiments E and F ($a_b = 1$), is more concentrated than in the experiments G and H. This strong initial concentration in experiment E is the cause of a high central accumulation of stars, and after some time favors the formation and maintenance of the bar. More precisely, it avoids a violently unstable solution, that will heat the disk and destroy the bar. In experiments G and H the bar forms more rapidly but it is not maintained. At t=80, 140 and 200 we observe that the gas in experiments E, G and H can reach the same maximum of density. While in experiment E the region out of the bar is depopulated from its gas, the contrary occurs in experiment F. In this experiment a strong central concentration of gas at the initial epochs together with a considerably lower concentration of stars induce the formation of an m=1 spiral mode in the central region of the

galaxy. The concentration of gas and stars is then almost completely stopped.
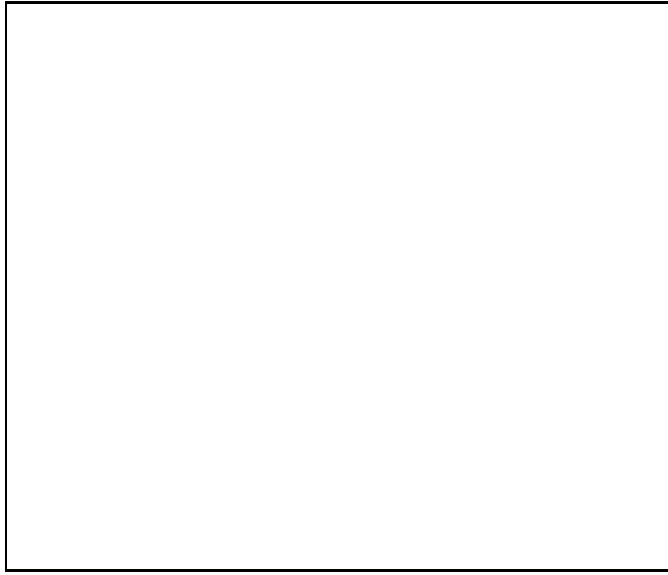
Fig. 9. Exp. E : the phase (in radian) of m=2 Fourier component for the stellar (left side) and the gaseous (right side) surface density and the total potential as a function of radius (in kpc) at four different epochs. Also shown is d_2, the amplitude of the m=2 component of the surface density of stars and gas. The scale of d_2 is in the right side.

We can observe that although the bar obtained in Exp. A shows approximately the same growth rate as that obtained in Exp. E, it is relatively longer. This is certainly due to the larger mass concentration of Exp. E, due to the gas dissipation. Also spiral structure is present in Exp. E in contrast to A, in the gas as well as in the stars. We remark also that there is a phase shift between the gas bar (leading) and that of the stars of approximately 30°in the first epochs. This explain the strong gravity torques exerted by the potential on the gas, which is driven inwards (cf Combes 1988). In her study about the secular evolution of spiral galaxies, Zhang (1995), suggested the existence of a collective dissipation mechanism responsible for the secular evolution of the stellar disks of spiral galaxies. Since the disk is not in complete equilibrium, there exists also a phase shift between the self-consistent spiral potential and the stellar density. This phase shift indicates that there is a torque applied by the spiral potential on the stars, and a secular transfer of energy and angular momentum between the stellar disk and the spiral density wave. In figure 9 we show, for experiment E, the phase of the m=2 Fourier component for the gas and stellar surface densities and for the total potential as a function of radius at four different epochs, t=20, 80, 140 and 200 (in 10^7 yrs). At the beginning (t=20) gaseous and stellar surface densities are in phase with the potential. See also in figure 2 the

agreement between the spiral arms developed in the gas and in the stars. At t=80, 140 and 200 there is in the gas a phase-shift between the surface density and potential, implying a large torque felt by the gas for a large range of the radii; after corotation, the stellar surface density leads the potential, while just before CR the potential leads the two components. Corotation is where the potential phase shows the maximum gradient. At t=200, a gas spiral feature just outside corotation introduces important phase shifts, but they are not related to the bar, as shown by d_2 the m=2 amplitude in the surface density.
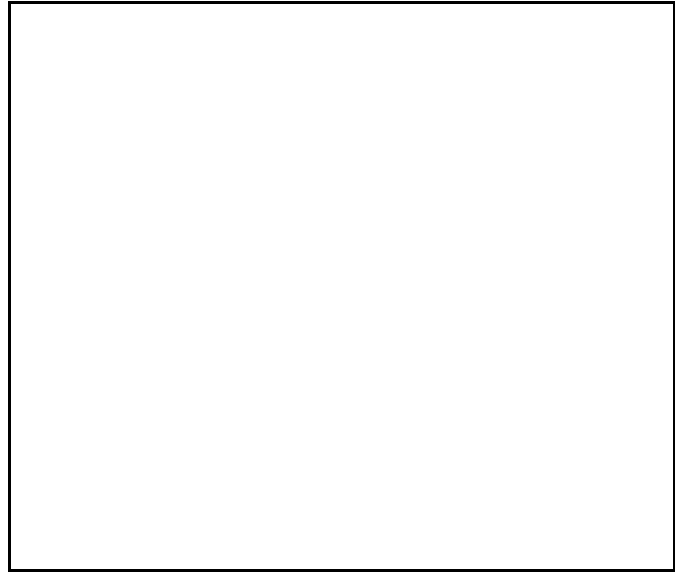
Fig. 10. Exp. I, E, and J: linear isodensity contours of stars and gas at epoch t=140 (in 10^7 yrs). X and Y are in kpc.

In order to probe the conditions required for the formation of a bar (as in experiment E) or an m=1 spiral mode (Exp. F), two other experiments (I and J) were done. In these experiments we used the same initial conditions for the stellar disk as in experiment E but the gaseous component has different degrees of concentration determined by the characteristic radius a_g. In figure 10 we compare the linear isodensity contours of the stars and gas at the time t=140 for Exp. I, E and J: when the gaseous disk is initially less concentrated a bar can form (Exp. J and E) while when it is initially more concentrated (Exp. I, $a_g = 4$) an m=1 spiral mode develops. In this latter case the stars and gas concentrations show a final behavior very different from that observed in the bar experiments. The results can be interpreted comparing the surface density of stars and gas at different epochs as shown in figure 11. Although the stellar density of Exp. I does not stand out from other experiments at any time, the gas density is different. While in Exp. E and J the bar forms, the concentration of gas increases and the region out of the bar is depopulated, in Exp. I, the development of an m=1 spiral

Fig. 11. Exp. E, I, and J : surface density (in code units) of stars and gas as a function of radius (kpc) at four different epochs, t=20, 80, 140 and 200 (in 10^7 yrs). The letters at the bottom left corner of each figure indicate (s) stars and (g) gas.

mode slows down the gas concentration. We discuss now in more details the formation of these m=1 spiral modes.

4. M=1 instabilities

Eccentric asymmetries in the distribution of light in spiral galaxies have been known for a long time (Baldwin et al. 1980; Wilson & Baldwin 1985). Lopsided features are preferentially observed in the distribution of gas in late-type spiral galaxies. In several cases these features can be identified as one-armed spirals (m=1 mode). More frequently, nuclei of galaxies are observed displaced with respect to the gravity center, as in M33 and M101 (de Vaucouleurs & Freeman 1970). Barred spiral galaxies can have their kinematical center displaced from the bar center (Christiansen & Jefferys 1976, Marcellin & Athanassoula 1982, Duval & Monnet 1985). The nucleus of M31 reveals such an off-centring (Bacon et al 1994) which has been interpreted in terms of an m=1 perturbation (Tremaine 1995). Miller & Smith (1992) have studied through N-body simulations of disk galaxies, a peculiar oscillatory motion of the nucleus with respect to the rest of the axisymmetric galaxy. They interpret the phenomenon as an m=1 instability, a density wave in orbital motion around the center of mass of the galaxy. Weinberg (1994) shows that a stellar system can sustain weakly damped m=1 mode for hundreds of crossing times. A fly-by encounter could excite such a mode, and explain off-centring in most spiral galaxies, or the forcing of a halo could maintain a time-dependent potential in the galaxy (Louis & Gerhard 1988).

In this section we concentrate on perturbations with azimuthal wavenumber m=1. The results of one of these simulations (Table 1, experiment F), which shows gravitational instabilities of this nature, is presented in figure 3. The linear isodensity contours of the gas show features in the central region that can be identified as an m=1 spiral mode. The Fourier analysis allows us to reconstruct the density distribution of the gas from the combination of the various components and single out the contribution of each one in the final configuration. In figure 12 we present the linear isodensity contours of the gas distribution reconstructed from the two main components (m=1 and m=2). Comparing figures 3 and 12 we can check the relative contribution of these components and how they add to each other.
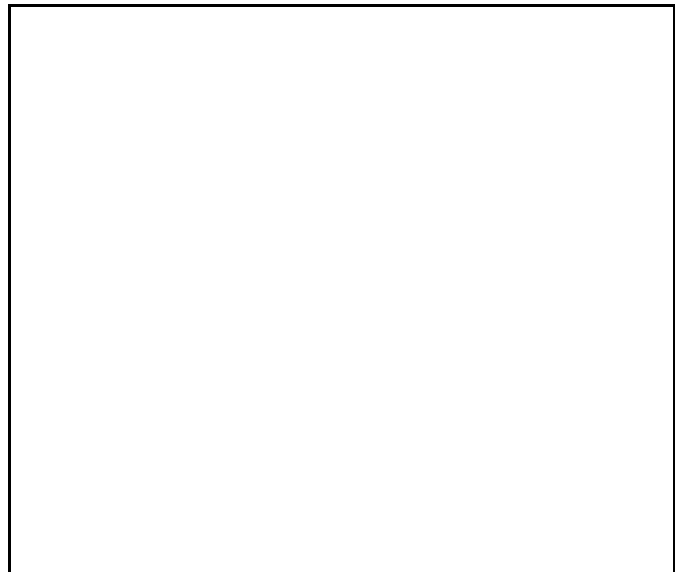
Fig. 12. Exp. F: linear isodensity contours do gas reconstructed from the m=1 and m=2 Fourier components epochs t=20, 80, 140 and 200 (in 10^7 yrs). X and Y are in kpc.

For this experiment, we have calculated the angular velocity $\Omega_p(r)$ of the m=1 wave. The m=1 wave is confined in the central region (r $\leq$ 3 kpc), with a pattern speed of the order of 400km/s/kpc. Figure 13 displays the Ω (solid curve), $\Omega + \kappa$ and $\Omega - \kappa$ (dashed curves) frequency curves, together with the expected position of the resonances (CR and OLR). The m=1 perturbation develops between the center of the galaxy and its OLR radius, slightly above 3 kpc. Outside this radius, independent perturbations, of symmetries m=1 and 2, develop (see figure 14. The pattern speed of these is of the order of 10-20 km/s/kpc. In figure 14 we show the linear isodensity contours of the gas in Exp. F at twelve consecutive epochs (from t=140 to 142.75, in 10^7 yrs). We can note that the central region (about 3 kpc around the densest cell) of the m=1 spiral wave rotates rapidly, completing almost two rotations
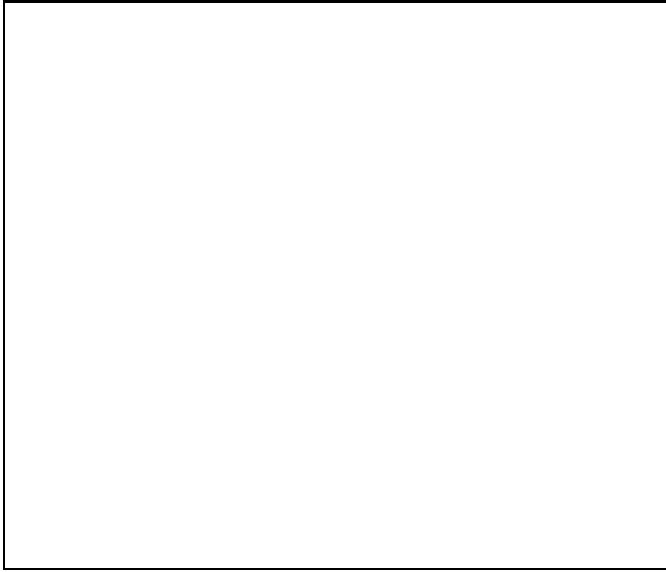
Fig. 13. Exp. F: The angular velocity $\Omega_p(r)$ of the m=1 wave and the frequency curves (in units of 100 km/s/kpc) as a function of radius (in kpc).

Fig. 14. Exp. F: linear isodensity contours of the gas at 12 close-by epochs (in 10^7 yrs). The circles show the region of 3 kpc around densest cell. The axis X and Y are in kpc.

during this time interval while the outer spiral structure evolves more slowly. The value of the central $\Omega_p(r)$, considerably greater than in the outer regions of the galaxy, precludes any non-linear coupling of the patterns in the two regions. In figure 15 we show the same linear isodensity contours displayed in figure 14 rotated with a constant angular velocity ($\Omega_p(r)$=400km/s/kpc). The position of the m=1 wave at each time in the central region confirms that the pattern speed is in fact considerably greater there.

It is important to remark that, at the initial instants of the simulation (t=20) in the central region (r=3 kpc), the mass of the gas increases to approximately 6 times its initial value, just before the appearance of the m=1 mode. After that, the growth rate of gas mass in this region slows down steadily with time. In the other experiments where the m=1 does not occur, the gas mass continues to grow rapidly. The slowing down of radial gas flow coincides also with a stabilisation of the gas angular momentum in the center, as soon as the m=1 arm is identified.

Adams et al (1989) have discovered numerically similar gravitational instabilities in gaseous disks associated with young stellar objects: eccentric m=1 modes, when the star did not lie at the center of mass of the system. Shu et al. (1990) presented an analytical description of a modal mechanism, the SLING amplification, or "Stimulation by the Long-range Interaction of Newtonian Gravity". This mechanism uses the corotation amplifier, where the birth of positive energy waves outside strengthens negative energy waves inside. In the SLING mechanism, a feedback cycle is provided by four waves outside corotation; long-trailing waves propagate from the OLR inward to the Q-barrier at CR where they refract in short trail-
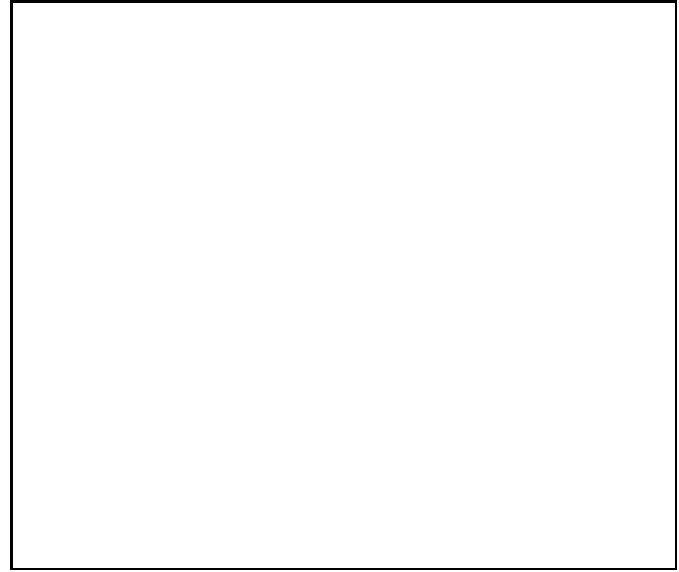

Fig. 15. The same linear isodensity contours of the gas at 12 close-by epochs (in 10^7 yrs) shown in figure 14 rotated of $\Omega_p(r) = 400$km/s/kpc.

ing waves. These propagate outwards, cross the OLR, and reflect back at the outer edge of the disk. This is a critical point, the whole amplification mechanism depends on the reflecting character of this outer edge. Then a short leading wave propagates inwards from the edge, through OLR, towards CR, where it refracts again into a long leading wave, that is then reflected at OLR. An essential point here is also the ability of waves not to be absorbed at OLR, that is why this mechanism apply to gaseous disks only.
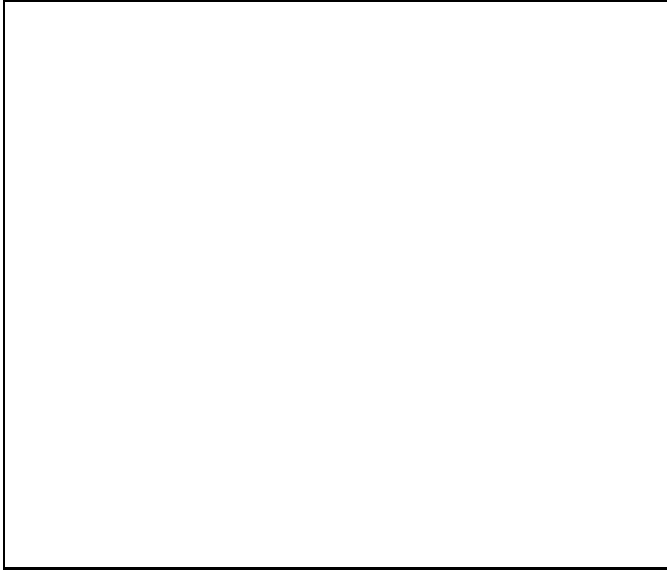
Fig. 16. Exp. F: position of the center of mass of the gas (circles) and the center of mass of the stars (*) relative to the center of mass of the system (crosses) calculated within radii from r=1 kpc to 10 kpc at different epochs indicated at the top left of each figure (in 10^7 yrs). X and Y are in kpc. The position of the center of mass of the gas and of the stars calculated within the same radius are connected by a straight line.
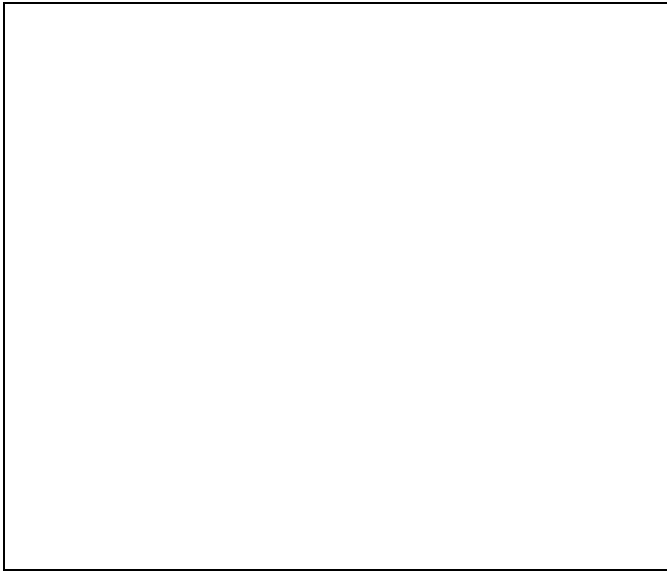

Fig. 17. Exp. E: position of the center of mass of the gas (circles) and the center mass of the stars (*) relative to the center of mass of the system (crosses) calculated inside radii from r=1 kpc to 10 kpc at different epochs indicated at the top of each frame (in 10^7 yrs). X and Y are in kpc.

Using a WKBJ analysis, they derived from the dispersion relation, and the condition of a constructive reflection, the required pattern speed for these modes. The instability arises uniquely from the displacement of the central star from the center of mass of the system, which creates an effective forcing potential. In our simulation the same effect is occurring, i.e. the center of mass of the gas and of the stars is displaced from the center of mass of the system and they are displace in opposite positions, inducing the m=1 wave formation. In other words, the modal mechanism proposed by Shu et al. (1990) may be in action in our experiment. In figures 16 and 17 we show the position of the center of mass of stars and gas calculated within radii from r=1 kpc to r=10 kpc, at 12 different epochs (indicated at the top left of each frame) for experiments F and E respectively. In this figures the circles indicate the position of the center mass of the gas, the symbol (*) the position of the center mass of the stars and the crosses the center mass of the system. From the comparison of figures 16 and 17, we note that when there is a bar (Exp. E) the position of the center of mass of the gas and of the stars agree with the position of the center mass of the system, while when an m=1 spiral wave is identified, the center of mass of the gas and of the stars are in opposite locations relative to the center of mass of the system.
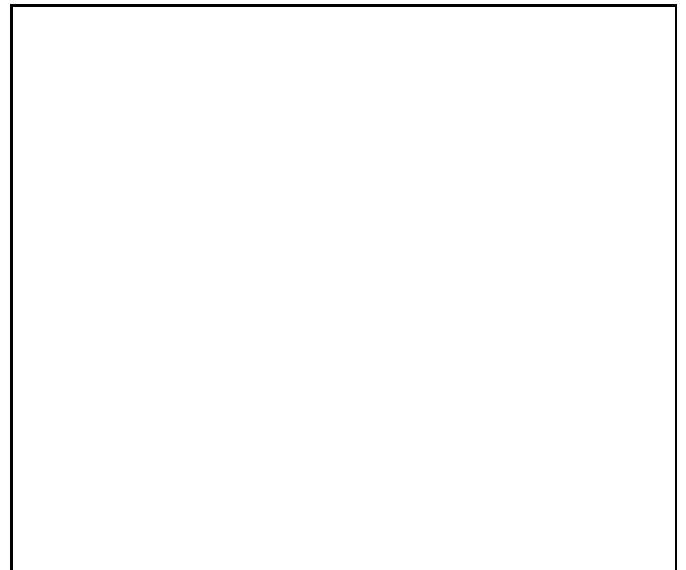

Fig. 18. Exp. F: Gray-colour maps do pattern speed $\Omega_p(r)$ (km/s/kpc) of the m=1 spiral wave determined from the total potential and from the surface density of the gas as a function of the radius (in kpc).

The power spectrum analysis, using the amplitude and the phase of the Fourier components of the total potential and of the surface density of the gas and of the stars, is another method that allow us to evidence the presence of the spiral modes in our simulations. This analysis give us

the pattern speed of all present spiral perturbations and their relative positions. The figure 18 displays gray-colour maps of the obtained angular velocity, from the potential and from the surface density of the gas (Exp. F) as a function of the radius, for the m=1 mode, using a such method. In these figure we can observe that the m=1 mode ($\Omega_p(r)$=400km/s/kpc), identified in the distribution of the gas density, it is more pronounced between the centre and the radius 3 kpc, extending however until the edge. The same behaviour can be verified in this figure for the potential, indicating that although this mode be more easily identified in the central region of the galaxy, it produces a perturbation in the total potential that extends until the edge.
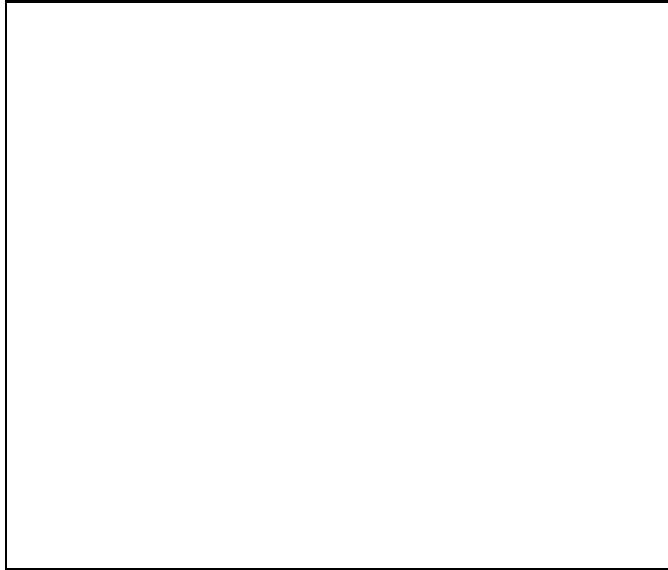

Fig. 19. Exp. F: the strength of the m=1 spiral perturbation p_1 as a function of time (in 10^7 yrs).

Figure 19 presents the strength of the m=1 (p_1) mode as a function of time. From this, we have computed the growth rate of the m=1 wave in the central region, assuming an exponentially growing mode. The growth time-scale obtained is approximately 3 t_d, at the radius of 3 kpc. This corresponds to the predictions of the SLING mechanism (Adams et al. 1989, Shu et al. 1990). Also, the fact that the m=1 behaviour described here occurs only when the gas mass fraction is high, is compatible with this mechanism, which is essentially gaseous in its origin.

5. Viscosity

The dynamical role of the dissipative gas component is essential to account for the variety of structures observed in spiral galaxies. But the actual amount of dissipation is not well known, and worries have been expressed that the numerical treatment of the gas component could in-
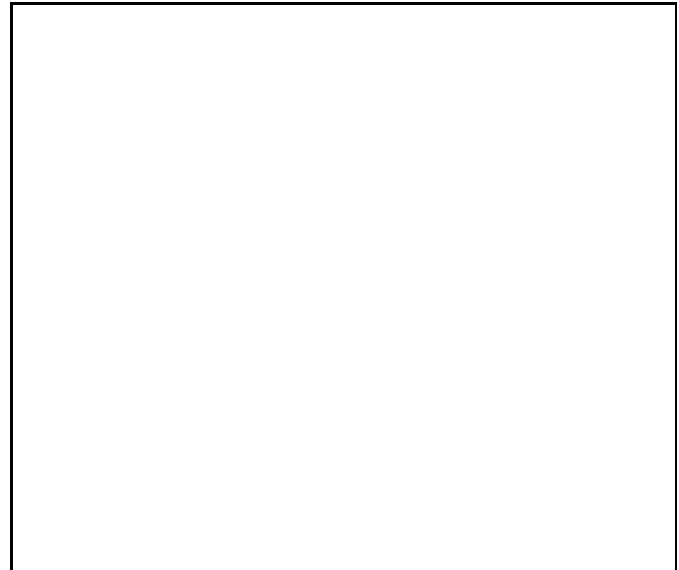
Fig. 20. Exp. F1: linear isodensity contours of the stars (left side) and gas (right side) at epochs t=20, 80, 140 and 200 (in 10^7 yrs). X and Y are in kpc.
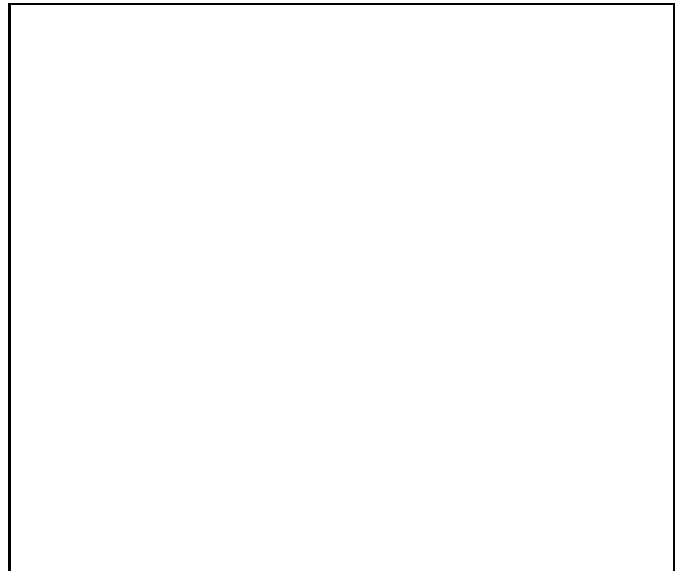

Fig. 21. Exp. F1: the strength of the m=1 spiral perturbation p_1 as a function of time (in 10^7 yrs). The m=1 strength has been averaged over radii 0 to 3 kpc.

troduce artificial angular momentum transfer, through a too large viscosity. In the real interstellar medium, the viscosity is due to macroscopic turbulent motions, that can be supersonic with a 10km/s velocity dispersion (e.g. Dickey et al 1990). But the corresponding viscous torques are quite weak at large-scale, and the time-scale for viscous transport of the galactic gaseous disk is larger than a Hubble time (e.g. Lin & Pringle 1987, Combes 1991). Gravitational torques are always dominant, and can trans-
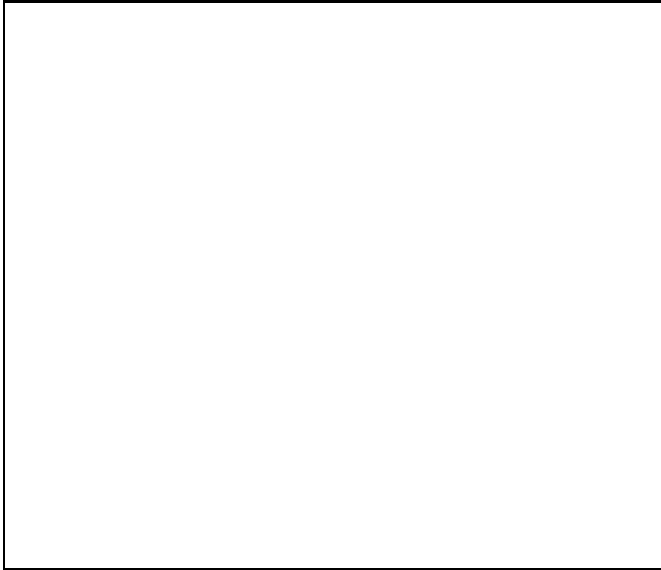
Fig. 22. Exp. F and F1 : surface density (in code units) of stars and gas as a function of radius (kpc) at four different epochs t=20, 80, 140 and 200 (in 10^7 yrs). The letters at the bottom left corner of each frame indicate (s) stars and (g) gas.

Fig. 23. Exp. F and F1 : radial velocity (top) and equivalent viscosity of the gas as a function of time (bottom), at radii 3, 7 and 11 kpc.

fer angular momentum on time-scales much shorter than the Hubble time. Fortunately, this makes gas-dynamical simulations more independent of the adopted physics of the interstellar medium.

We therefore would like to check that the beam-scheme used here does not introduce too large viscous torques. In order to evaluate quantitatively the numerical viscosity of the method we have carried out further control experiments. The artificial viscosity must be proportional to the size of the grid cell where the surface density is computed. In the experiment F1 we have used the same initial conditions as in experiment F but the grid is now composed of four times more cells (512×512 cells) with four times smaller surface each. In figure 20 we present the linear iso-density contours of the stars and gas for Exp. F1 at four different epochs. As described above for the former experiments, we calculate for experiment F1 the growth rate of the m=1 spiral mode from the time evolution of its amplitude p_1 plotted in figure 21. The corresponding growth time-scale is approximately 23 t_d, i.e. in this experiment the m=1 spiral mode needs a much longer time-scale to develop, compared to Exp. F. The analysis of the surface density distribution of stars and gas as a function of radius and at different epochs, as shown in figure 22, shows that although initially (t=20) the viscosity is larger in Exp. F, driving a higher gas flow towards the center, at following epochs (t=80) the surface density distributions of Exp. F and F1 evolve in a similar manner. After that, from t=100, their behavior diverge from one another. At t=140, the gas density is more concentrated in Exp. F1, although the numerical viscosity is there lower. This must be due to the
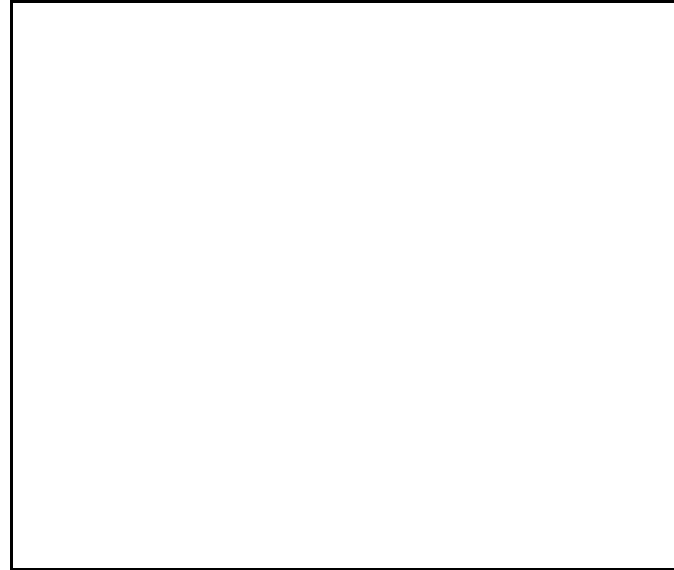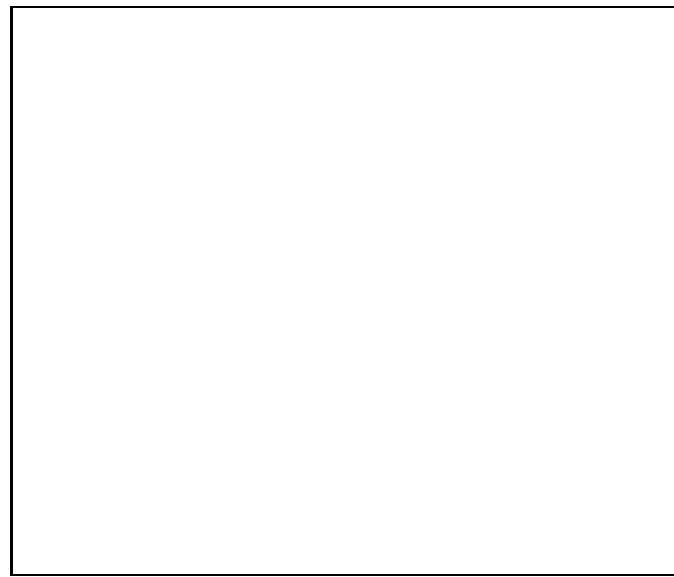

Fig. 24. Exp. F and F1 : radial velocity (top) and equivalent viscosity of the gas as a function of radius (bottom), at epochs t=20, 80, 140 and 200 (in 10^7 yrs).

fact that the m=1 arrived later, so the gravity torques had more time to act than in Exp. F.

In order to interpret this behavior, we calculated the equivalent "gravitational viscosity" of the gas as proposed by von Linden et al. (1995). From this point of view, the combination of gas dissipation and gravity torques from non-axisymmetric gravitational instabilities developing in the disks, is considered as an equivalent "gravitational viscosity". The gravity torques produce an angular-

momentum re-distribution and an evolution of the surface density of the gas. By monitoring this surface density one can derive the equivalent viscosity quantitatively. This "gravitational viscosity" does not correspond to a classical gaseous viscosity, but it is a measure of the efficiency with which gravity torques transfer angular momentum outward and matter inward in the system. In figure 23 is plotted (at top) the behavior of the radial velocity of the gas as a function of time at three different radii (3, 7 and 11 kpc) for experiments F and F1 and (at bottom) the behavior of the corresponding "gravitational viscosity". For experiment F the viscosity has a positive value initially, just before the development of the m=1 perturbation, and converges later on towards a zero mean value. In experiment F1, the viscosity remains large for a longer time, which corresponds to the delay in the development of the m=1 perturbation with respect to Exp. F. To better visualize the viscosity behavior in these experiments, we show in figure 24 the radial velocity and the gravitational viscosity as a function of radius at four different epochs. While the viscosity in Exp. F is negative at the center and tends to zero at larger radii after the development of the m=1 mode, in experiment F1 the viscosity remains positive.

In summary, although the numerical viscosity is slightly higher in Exp. F, this is largely compensated by the larger gravitational viscosity observed in Exp. F1. When the grid cells are smaller, the gas can condense in cold clumps more easily (see fig 20), and the lumpiness of the gas has a significant gravitational effect. Although the numerical viscosity in itself does not alter significantly the results, the dynamic range and spatial scale of gaseous condensations, and therefore the physics of the ISM, plays a significant role.

6. Summary and Conclusions

We have investigated the role of gas dynamics in the gravitational instabilities of galaxy disks, through self-gravitating simulations of the coupled stellar and gaseous components. In the present paper, we have focussed on the diffuse gas component, that can be considered as a fluid, subject to pressure forces and shocks.

Spiral structure is only transient in purely stellar disks. In the absence of a cooling mechanism the disk is heated by the gravitational instabilities themselves, and reaches a hot steady-state, that prevents the development of new instabilities. If a bar has developed, it can remain for a Hubble time. In presence of gas, even with as low a mass fraction as a few percents, the disk is continuously cooled down, and responsive to new dynamical instabilities. Due to its dissipative character, the gas acts as a regulator. If its conversion into stars and its continuous accretion is considered, the gas can prolong the phase of dynamical instability to more than a Hubble time, which can account

for the spiral density waves observed in so many spiral galaxies.

Dynamical instabilities play themselves a self-regulating role, since the bar gravity torques drive the gas towards the center, and a sufficiently massive central condensation begins to dissolve the bar. Also, above a certain central gas concentration, a one armed spiral structure can develop, which stops or slows down the radial gas flow and the angular momentum transfer. We have studied the conditions required for the m=1 mode appearance, its pattern speed and extension. The m=1 perturbation is confined in the central part of the galaxy, and is noticeable only within its own outer Lindblad resonance. Its angular speed is more than 10 times the speed of the external perturbations. It appears to have a purely gaseous origin, and corresponds to the phenomenon identified in protostellar disks by Adams et al. (1989). The mode grows in a few dynamical time-scales as predicted for the SLING mechanism of Shu et al. (1990). There is evidence from our simulations that stars and gas are off-centered with respect to the center of mass of the system, which indicates that this mechanism could be at work.

References

Adams F. C., Ruden S. P., Shu F. H., 1989, ApJ 347, 959.
Athanassoula E., Sellwood J.A., 1986, MNRAS 221, 213
Bacon R., Emsellem E., Monnet G., Nieto J-L., 1994, A&A 281, 691
Baldwin J. E., Lynden-Bell D., Sancisi R., 1980, MNRAS 193, 313.
Bertin G., Romeo A.B.: 1988 A&A 195, 105
Binney J. & Tremaine S., 1987, in Galactics Dynamics, Princeton University Press, Princeton, New Jersey
Birdsall C. K. & Fuss D., 1969, J. Comput. Phys. 3, 494.
Christiansen J.H., Jefferys W.H., 1976, ApJ 205, 52
Combes F. & Gerin M., 1985, A&A 150, 327.
Combes F., 1988, in "Galactic & Extragalactic Star Formation", Nato Advanced Studies Series, ed. R.E. Pudritz & M. Fich, Kluwer p. 475
Combes F., Debbasch F., Friedli D., Pfenniger D., 1990, A&A 233, 82
Combes F., 1991, in "Dynamics of Galaxies and their Molecular Cloud Distribution", ed. F. Combes & F. Casoli, IAU 146, 255 (Kluwer)
Contopoulos G., Gottesman S. T., Jr. Hunter J. H., England M. N., 1989, ApJ 343, 608.
de Vaucouleurs G., Freeman K.C., 1970, IAU 38, 356
Dickey J.H., Hanson M.M., Helou G., 1990, ApJ 352, 522
Duval M.F., Monnet G., 1985, A&AS 61, 141
Elmegreen B. G., 1994, ApJ. 427, 384
Friedli D., Benz W., 1993, A&A 268, 65
Friedli D., Martinet L., 1993, A&A 277, 27

Hasan H. & Norman C., 1990, ApJ 361, 69.

Huntley J. M., Sanders R. H., Roberts W. W., 1978, ApJ 221, 521.

Jog C.J., Solomon P.M., 1984, ApJ 276, 114

Lin D.N.C, Pringle J.E., 1987, MNRAS 225, 607

Louis P.D., Gerhard O.E., 1988, MNRAS 233, 337

Marcelin M., Athanassoula E., 1982, A&A 105, 76

Miller R.H., Smith B.F., 1992, ApJ 393, 508

Ostriker J.P., Peebles P.J.E., 1973, ApJ 186, 467

Phinney E. S., 1994, in Mass Transfer Induced Activity in Galaxies, ed. I. Shlosman (Cambridge Univ. Press), p.1.

Prendergast K., 1983, in IAU Symposium 100, Internal Kinematics and Dynamics of Galaxies, ed. E. Athanassoula (Dordrecht:Reidel), p.215.

Roberts W. W. Huntley J. M., van Albada G. D., 1979, ApJ 233, 67.

Roberts W. W. & Hausman M. A., 1984, ApJ 277, 744.

Sanders R. H. & Prendergast K. H., 1974, ApJ 188, 489.

Sanders R. H. & Tubbs A. D., 1980, ApJ 235, 803.

Schwarz M. P., 1981, ApJ 247, 77.

Schwarz M. P., 1984, MNRAS 209, 93.

Sellwood J.A., Carlberg R.G., 1984, ApJ 282, 61

Sellwood J.A., Wilkinson A., 1993, Rep. Prog. Phys., 56, 173

Shlosman I. & Noguchi M., 1993, ApJ 414, 474.

Shu F. H., Tremaine S., Adams F. C., Ruden S. P., 1990, ApJ 358, 495.

Toomre A., 1962, ApJ 138, 385.

Toomre A., 1964, ApJ 139, 1217

Tremaine S., 1995, AJ 110, 628

van Albada T. S. & Sanders R. H., 1982, MNRAS 201, 303.

van Albada G. D., 1983, in IAU Symposium 100, Internal Kinematics and Dynamics of Galaxies, ed. E. Athanassoula (Dordrecht:Reidel), p.237.

von Linden S., Lesch H., Combes F., 1995, A&A preprint.

Weinberg M.D., 1994, ApJ 421, 481

Wilson A. S. & Baldwin J. A., 1985, ApJ 289, 124.

Zhang X., 1995, ApJ preprint.